Mixed convection in turbulent particle-laden channel flow at Re = 180

Mixed convection in turbulent particle-laden channel flow at Re_τ = 180

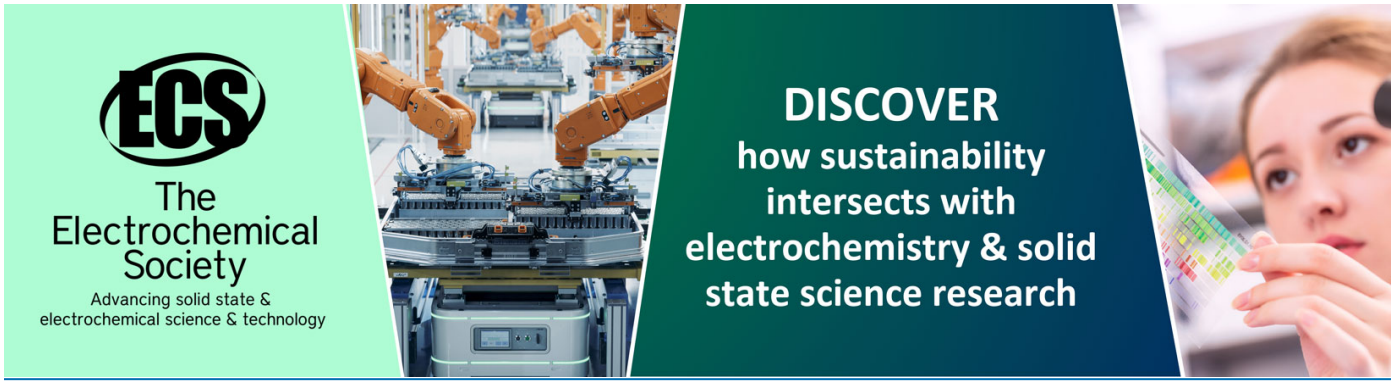

Mixed convection in turbulent particle-laden channel flow at $\mathbf{Re}_{\boldsymbol{\tau}} = \mathbf{180}$

D Zaza[1,*] and M Iovieno[1]

[1] Dipartimento di Ingegneria Meccanica e Aerospaziale, Politecnico di Torino, Corso Duca degli Abruzzi 24, 10129 Torino, Italy

* Corresponding author: domenico.zaza@polito.it

Abstract. A numerical investigation of mixed convection in a turbulent particle-laden channel flow is presented. Using Eulerian-Lagrangian Direct Numerical Simulations (DNSs) within the point-particle approach, the interaction between wall turbulence, particle inertia and thermal inertia, and buoyancy in the two-way coupling regime has been studied. The flow dynamics is controlled by the friction Reynolds number, Richardson number, particle Stokes and thermal Stokes numbers, and the Prandtl number. The effects of particle inertia and buoyancy on fluid and particle statistics are shown for a friction Reynolds number of 180, Stokes numbers ranging from 0.6 to 120, Richardson numbers ranging from 2.72×10^{-4} to 27.2 at a single Prandtl number, 0.71. The results indicate that the effect of particle inertia is significant on particle statistics, but not as pronounced on fluid statistics at the relatively low volume fraction considered. Particle inertia modulates the overall heat flux in a non-monotonic way.

1. Introduction

Particles suspended in turbulent flows are a common occurrence in many natural and industrial processes. Natural examples include the transport and deposition of aerosols, the formation of droplets in clouds, sand and dust storms, volcanic eruptions, soil erosion processes, and sediment transport in watercourses. On the other hand, engineering processes such as pharmaceutical sprays, liquid fuel combustion, and combustion in solid propellant endoreactors also involve particle-laden flows. Direct Numerical Simulation (DNS) has become the main tool for improving the physical understanding of these flows due to recent advances in high-performance computing. This approach allows for the study of the details of the flow, which are often difficult to observe experimentally, particularly when additional physical phenomena such as heat transfer, buoyancy, mass transfer due to condensation or evaporation, chemical reactions, and acoustic waves play a role. When the particle size is smaller than the Kolmogorov scale, the Lagrangian point-particle method is the most commonly used approach [1]. In this approach, particles are treated as point-like, and their dynamics is determined by solving a set of ordinary differential equations for each particle. This method reduces the computational burden as it does not require the detailed simulation of the flow around each particle. Over the past fifty years, since the pioneering work by [2], point-particle DNS has allowed for the simulation of very large numbers of particles in different flow configurations, leading to fundamental insights into the subject. In inhomogeneous turbulent flows, for example, the phenomenon of preferential concentration of particles, known as turbophoresis, is crucial [3]. Particles tend to migrate from regions of high turbulence intensity toward lower-intensity regions due to the property of inertial particles to disperse more quickly where the turbulent intensity is higher. In particular, in wall-bounded flows, large-scale clustering and

preferential concentration of particles are observed in the near-wall region [4] and are strongly influenced by the local Stokes number [5]. However, this phenomenon is weakened in the two-way coupling regime, i.e. when the full momentum exchange between the two phases is taken into account, as a consequence of the damping performed by the particles on the wall-normal and spanwise velocity fluctuations. Indeed, for particle volume fractions greater than 10^{-6}, the modulating effects of particles on turbulence cannot be neglected [6]. In this regime, the momentum and heat exchange between the phases has to be taken into account. Inertial particles have been found to enhance heat transfer as their thermal inertia grows [7], while they tend to suppress fluid temperature increments as the particle thermal response time increases [8].

Mixed convection occurs when both forced convection (driven by a pressure gradient) and natural convection (driven by buoyancy forces) are present in a fluid flow, and can significantly impact on the fluid flow and, consequently, the heat transfer characteristics of a system. The presence of particles can further modulate the flow, due to the interplay between preferential concentration and small-scale features. While there has been research on both particle-laden flows and mixed convection flows separately, to the best of our knowledge, the combination of the two phenomena has not been widely explored for finite inertia particles. All studies focus on nanoparticles and use a single-phase Eulerian approach or a two-phase Eulerian-Eulerian method, which can provide a description of the flow only for very small Stokes numbers [9]. Investigating the combined effects of these two phenomena could lead to a better understanding of the complex behaviour of particle-laden flows in both nature and industrial processes. In this exploratory study, we used Lagrangian-Eulerian direct numerical simulations to evaluate the role of particles with finite thermal inertia on the mixed convection in an horizontal channel flow heated from below.

2. Physical model

In this section, we present the physical model for the non-isothermal particle-laden flow in an horizontal plane channel, when heat transfer by natural convection is also considered. A phase consisting of small (sub-Kolmogorov), heavy, spherical, and collisionless particles is dispersed in the fluid. The Eulerian-Lagrangian approach is adopted: the continuous phase is described in an Eulerian way, whereas the dispersed phase is followed in a Lagrangian way, solving a set of equations for each particle. The two-way coupling between particles and fluid is here considered for both the momentum and the internal energy.

The flow is driven by a uniform pressure gradient parallel to the walls, which defines the streamwise direction, and is subject to buoyancy effects due to a temperature difference between the upper and lower walls combined with a uniform wall-normal gravitational field. The temperature is considered uniform over each wall, with the bottom wall warmer and the upper wall colder to obtain an unstable stratification, as in [10]. Computationally, the flow is solved in a parallelepiped domain, with size $2\pi h$ in the streamwise direction x, $2h$ in the wall normal direction y, and $2\pi h$ in the spanwise direction z, where h is the channel half-height. Periodicity is imposed in the streamwise and spanwise directions, exploiting the statistical homogeneity in these directions, while at the walls fluid velocity satisfies no-slip conditions and the temperature is set equal to the wall temperature. Since the flow is driven by both the mean pressure gradient, $\partial\langle p\rangle/\partial x$, and the temperature difference, $T_1 - T_2$, between the lower and upper walls, the equations are made dimensionless using h as the reference length-scale, the friction velocity $u_\tau = [(h/\rho)\,|\partial\langle p\rangle/\partial x|]^{1/2}$ as the reference velocity scale, the carrier flow mean density as the density (and mass) reference, and the half temperature difference $(T_1 - T_2)/2$ as the reference temperature variation. The governing equations are detailed below in dimensionless form; all variables denote dimensionless quantities unless explicitly stated.

2.1. Fluid phase

The fluid phase is governed by the incompressible Navier-Stokes equations with an advection-diffusion equation for the fluid temperature. Momentum and temperature are coupled by buoyancy forces through

the usual Boussinesq approximation, so that the fluid phase is governed by the following equations in tensorial notation ($x_1 = x, x_2 = y, x_3 = z$),

$$\frac{\partial u_j}{\partial x_j} = 0, \tag{1}$$

$$\frac{\partial u_i}{\partial t} + \frac{\partial \left(u_i u_j\right)}{\partial x_j} = -\frac{\partial p}{\partial x_i} + \frac{1}{\mathrm{Re}_\tau}\frac{\partial^2 u_i}{\partial x_j^2} + \mathrm{Ri}_\tau \vartheta \delta_{i,2} + \delta_{i,1} - C_{u,i}, \tag{2}$$

$$\frac{\partial \vartheta}{\partial t} + \frac{\partial \left(\vartheta u_j\right)}{\partial x_j} = \frac{1}{\mathrm{Re}_\tau \mathrm{Pr}}\frac{\partial^2 \vartheta}{\partial x_j^2} - C_\vartheta. \tag{3}$$

Here, $u_i(t, \boldsymbol{x})$ is the i-th component of the fluid velocity field, $p(t, \boldsymbol{x})$ stands for the fluctuating pressure field, and $\vartheta(t, \boldsymbol{x})$ is the temperature field. In this form, the wall boundary conditions for the dimensionless temperature are $\vartheta(t, x, \pm 1, z) = \mp 1$. The three non-dimensional governing parameters arising from the choice of reference scales are the friction Reynolds number, $\mathrm{Re}_\tau = u_\tau h/\nu$, the Prandtl number, $\mathrm{Pr} = \nu/\kappa$, and the friction Richardson number, $\mathrm{Ri}_\tau = h\alpha g \Delta T_{\mathrm{ref}}/u_\tau^2$, where g is the gravity acceleration and ν, κ and α are respectively the kinematic viscosity, the thermal diffusivity, and the thermal expansion coefficient of the fluid. Thus, the term $\mathrm{Ri}_\tau \vartheta \delta_{i,2}$ in equation (2) represents the net buoyancy force acting against the gravitational field. Finally, the terms $C_{u,i}$ and C_ϑ are the particle feedback on the momentum and the internal energy of the carrier phase, which will be soon discussed.

2.2. Dispersed phase

We consider the flow seeded with N_p identical, rigid, small, heavy, and spherical particles, with radius r much smaller than any flow length scale. In such a situation, particle dynamics is described using a Lagrangian approach, where the position, velocity, and temperature of each particle are determined by external forces and heat exchanged with the carrier fluid. The equations of motion for a spherical particle in a fluid flow were formulated by Maxey and Riley in [11], where it was shown that for particle densities much larger than that of the fluid, only the Stokes drag force needs to be considered, with the added mass, Basset history, and pressure gradient forces being negligible. To avoid sedimentation, no buoyancy is considered for particles. The motion of the j-th particle is described by the dimensionless equations:

$$\frac{\mathrm{d}\boldsymbol{x}_j}{\mathrm{d}t} = \boldsymbol{v}_j(t), \qquad \frac{\mathrm{d}\boldsymbol{v}_j}{\mathrm{d}t} = \frac{\boldsymbol{u}\left(t, \boldsymbol{x}_j\right) - \boldsymbol{v}_j(t)}{\tau_u}\left(1 + 0.15\ \mathrm{Re}_j^{0.687}\right), \tag{4}$$

where $\boldsymbol{x}_j(t)$ and $\boldsymbol{v}_j(t)$ denote respectively the position and velocity of the particle, $\boldsymbol{u}(t, \boldsymbol{x}_j)$ is the fluid velocity at the particle position and time, and τ_u is the particle relaxation time, given in dimensionless form by

$$\tau_u = 2/9\ \rho_p r^2 \mathrm{Re}_\tau. \tag{5}$$

The term within parenthesis in equation (4) represents a semiempirical correction to the Stokes drag coefficient devised in [12] for spherical particles. This correction is based on the Reynolds number of the fluid-particle relative motion, $\mathrm{Re}_j = 2r\left|\boldsymbol{u}\left(t, \boldsymbol{x}_j\right) - \boldsymbol{v}_j(t)\right|\mathrm{Re}_\tau$.

An equation for the temperature of the j-th particle, ϑ_j, can be obtained applying the first law of thermodynamics to the particle, and assuming quasi-steady conduction and convection over particle scale as the main mechanisms through which heat is transferred between the two phases:

$$\frac{\mathrm{d}\vartheta_j}{\mathrm{d}t} = \frac{\vartheta\left(t, \boldsymbol{x}_j\right) - \vartheta_j(t)}{\tau_\vartheta}\frac{\mathrm{Nu}_j}{2}. \tag{6}$$

Here, the particle Nusselt number, Nu_j, is given by the correlation introduced in [13] for a spherical particle:

$$\mathrm{Nu}_j = 2 + 0.6\,\mathrm{Re}_j^{1/2}\mathrm{Pr}^{1/3}. \tag{7}$$

Similarly to τ_u, the quantity τ_ϑ is the particle thermal relaxation time. In dimensionless form, it is given by

$$\tau_\vartheta = 1/3\;\rho_p c_p r^2 \mathrm{Re}_\tau \mathrm{Pr}, \tag{8}$$

where c_p is the particle specific heat, normalized with the fluid specific heat at constant pressure. The relaxation times τ_u and τ_ϑ describe particle inertia and thermal inertia, and their ratios with the fluid flow scales, called Stokes numbers, determine their dynamics [1]. In a turbulent flow, the most important flow timescale for particle motion is the smallest one, which in a turbulent wall bounded flow is the viscous timescale. In dimensionless form, it is $\tau_\eta = 1/\mathrm{Re}_\tau$, so that the particle Stokes number and thermal Stokes number are defined as

$$\mathrm{St} \coloneqq \frac{\tau_u}{\tau_\eta} = \frac{2}{9}\rho_p r^2 \mathrm{Re}_\tau^2, \qquad \mathrm{St}_\vartheta \coloneqq \frac{\tau_\vartheta}{\tau_\eta} = \frac{1}{3}\rho_p c_p r^2 \mathrm{Re}_\tau^2 \mathrm{Pr}. \tag{9}$$

Particle-particle interactions are disregarded, and elastic collisions are assumed when particles hit the walls. Moreover, if a particle leaves the domain through a periodic boundary, it is reintroduced at the opposite side with the same velocity and temperature. When the volume fraction is above 10^{-6}, particle feedback on the carrier flow, represented by $\boldsymbol{C}_u$ and C_ϑ in equations (2) and (3) cannot be neglected. These terms are equal to the momentum and heat exchanged per unit volume by all the N_p particles with the fluid, so that, for point particles they have the following form:

$$\boldsymbol{C}_u = \frac{4}{3}\pi\rho_p r^3 \sum_{j=1}^{N_p} \frac{\mathrm{d}\boldsymbol{v}_j}{\mathrm{d}t}\delta(\boldsymbol{x}-\boldsymbol{x}_j), \qquad C_\vartheta = \frac{4}{3}\pi\rho_p c_p r^3 \sum_{j=1}^{N_p} \frac{\mathrm{d}\vartheta_j}{\mathrm{d}t}\delta(\boldsymbol{x}-\boldsymbol{x}_j). \tag{10}$$

The time derivatives $\mathrm{d}\boldsymbol{v}_j/\mathrm{d}t$ and $\mathrm{d}\vartheta/\mathrm{d}t$ are given by equations (4) and (6), respectively.

3. Numerical method

The carrier flow equations (1-3) are solved using the formulation proposed by [14], which is convenient because the Poisson equation for the pressure field does not need to be solved. This formulation uses the wall-normal component of the vorticity vector, $\eta = \partial u/\partial z - \partial w/\partial x$, and the wall-normal component of the velocity field, v, as main variables which are advanced in time, and reformulates continuity and momentum equations as a second order equation for η and a fourth order equation in v. The equations for the fluid phase are discretized in space using a pseudo-spectral method: the Fourier-Galërkin approach is applied in the two homogeneous directions x and z, whereas the Chebyshev-tau method is used to treat the wall-normal direction y. The convective non-linear terms are computed pseudo-spectrally using a de-aliasing procedure based on the 2/3-rule. Time advancement of the fluid equations is performed using the explicit two-step Adams-Bashforth scheme for the convective, the particle feedback, and the buoyancy terms, and an implicit Crank-Nicolson scheme for the diffusive terms. The application of these schemes, along with the Influence Matrix method [15], reduces the problem of determining the velocity and the temperature fields to solving, at each time-step and for each couple of Fourier modes, three one-dimensional Helmholtz equations for η, $\varphi = \nabla^2 v$, and ϑ. The Chebyshev-tau scheme applied to these equations leads to quasi-tridiagonal algebraic systems in which the coefficients of the even and the odd Chebyshev polynomials are decoupled [16]. Thus, each algebraic system can be split in two smaller problems which are solved by means of the Thual algorithm [17]. Then, v is determined from $\varphi = \nabla^2 v$ exploiting the Influence Matrix method, and u and w are obtained from η and the incompressibility constraint. Finally, the equations for the mean flow in the streamwise

and the spanwise directions are solved. Equations (4) and (6) describing particle dynamics are integrated in time using the same Adams-Bashforth scheme employed for the fluid phase. The evaluation of the fluid velocity and temperature at the particle location is carried out through a tri-linear interpolation, while the feedback terms are evaluated through the tri-linear projection onto the eight grid points of the computational cell the particle belongs to.

4. Results and discussion

In order to analyse the role of particles in mixed convection, we conducted eighteen simulations on a 192×201×192 grid in the streamwise, wall-normal and spanwise directions. These simulations were performed using a constant friction Reynolds number ($\mathrm{Re}_\tau = 180$) and a given Prandtl number ($\mathrm{Pr} = 0.71$). The resolution is therefore $\Delta x^+ = \Delta z^+ \simeq 5.9$, and Δy^+ between 0.02 and 2.9. The number of particles ($N_p = 11{,}782{,}400$) and the particle non-dimensional radius ($r = 4 \times 10^{-4}$) were fixed, resulting in a volume fraction equal to 4×10^{-5}. Different Stokes numbers were obtained by changing particle density. The simulations can be categorized into three groups. The first group involved simulating the unladen flow, considering both forced convection and mixed convection for five friction Richardson numbers ranging from 2.72×10^{-4} to 27.2. These simulations served as benchmarks to assess the influence of particles on the flow. The second group consisted of simulations of the two-way coupled particle-laden flow, considering three different Stokes numbers: $\mathrm{St} = 0.6$, 60, and 120. Since the ratio between the specific heats of the two phases ($c_p = 4.17$) remained constant, the ratio between the thermal Stokes number and the Stokes number also remained constant. These simulations exclusively accounted for forced convection ($\mathrm{Ri}_\tau = 0$). Finally, in the third group, we examined the combined effect of mixed convection and particle inertia by conducting nine particle-laden flow simulations with two-way coupling. These simulations considered three friction Richardson numbers (2.72×10^{-2}, 2.72×10^{-1}, 2.72) and three Stokes numbers ($\mathrm{St} = 0.6$, 60, 120).

Figure 1 illustrates the impact of mixed convection on the unladen channel flow. For friction Richardson numbers below one, the influence of natural convection on the mean flow and mean temperature field is negligible. The curves closely align with the reference curve, which corresponds to the case of forced convection ($\mathrm{Ri}_\tau = 0$). However, as the value of Ri_τ exceeds one, natural convection becomes more significant, leading to a substantial change in the flow structure. Out of the wall layer ($y^+ > 30$), the mean streamwise velocity increases for $\mathrm{Ri}_\tau = 2.72$ and then decreases for $\mathrm{Ri}_\tau = 2.72 \times 10^1$ compared to the reference case. Throughout the range of $30 < y^+ < 120$, a recognizable logarithmic law of the form $\langle u \rangle = 1/k \log y^+ + B$ is still observed for all cases, with the exception of $\mathrm{Ri}_\tau = 2.72$, where no clear logarithmic layer can be identified. When data are fitted with a logarithmic profile, for $\mathrm{Ri}_\tau < 1$ we obtained $k \simeq 0.393$ and $B \simeq 5.335$, the classical values of the coefficients in a boundary layer, while for $\mathrm{Ri}_\tau = 27.2$, we obtained $k \simeq 0.626$ and $B \simeq 8.346$. The presence of natural convection is also evident in the abrupt change of the mean temperature profile (figure 1(b)) and temperature variance profile (figure 1(d)). Natural convection flattens the mean temperature profile in the central region of the channel, confining temperature gradients to a narrower zone near the walls, whose thickness reduces with Ri_τ. Furthermore, for the two highest simulated Ri_τ values, an inflection point with negative temperature gradients is observed near the centerline of the channel, as reported in [18] for Ri_τ values of 10^2 and 10^3. The temperature variance profile (figure 1(d)) confirms this abrupt change in flow regime. In the $\mathrm{Ri}_\tau < 1$ range, the temperature variance exhibits a maximum at the center of the channel and a secondary peak at $y^+ \simeq 20$, in the upper region of the buffer layer. As the influence of natural convection increases, the temperature variance at the center decreases and the curve flattens, while the intensity of the peak near the wall grows, shifting closer to the wall. When natural convection dominates over forced convection, the temperature variance decreases throughout the channel, and the peak further migrates toward the wall. For higher Richardson numbers, the trend of the temperature variance is expected to approach that of pure Rayleigh-Bénard flow. Figure 1(c) presents the wall-normal temperature-velocity correlation, which is directly proportional to the convective heat flux by turbulent fluctuations in the y-direction.

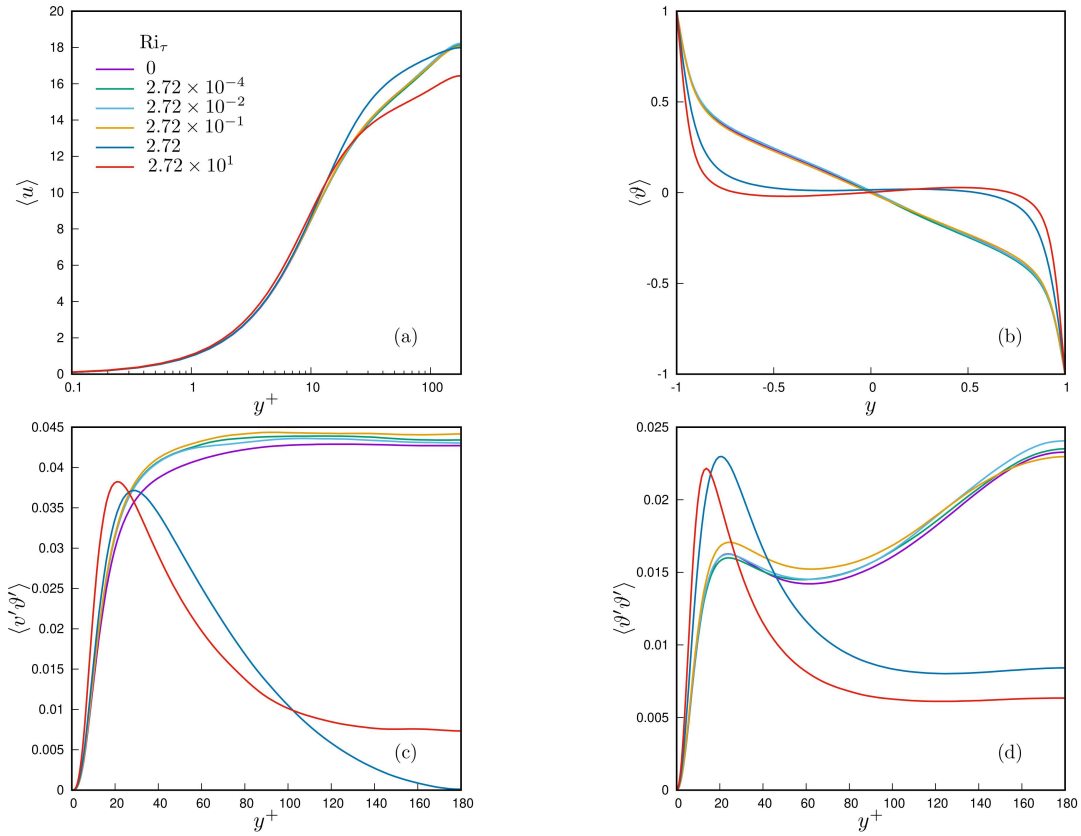

Figure 1. Unladen flow, effect of the Richardson number, Ri_τ, on flow statistics: (a) mean streamwise velocity, (b) mean temperature, (c) wall-normal turbulent transport, (d) temperature variance.

Figure 2 illustrates the particle and flow statistics obtained from a two-way coupled particle-laden flow, focusing specifically on forced convection conditions. Due to the relatively low particle volume fraction of 4×10^{-5}, the influence of particle inertia on flow statistics is not as significant as on particle statistics, in agreement with existing literature [1]. One notable effect observed is turbophoresis, as revealed by the concentration profiles (figure 2(b)). The concentration of particles normalized with the mean concentration exhibits a maximum in the viscous sublayer ($y^+ < 5$), which strengthens and moves towards the wall as the Stokes number increases from 0.6 to 60. This behavior is expected since particle inertia becomes more pronounced, leading to enhanced particle accumulation near the wall. However, it is important to note that the trend of the maximum concentration is non-monotonic: as particle inertia further increases and the Stokes number reaches 120, the maximum concentration decreases. This reduction can be attributed to the damping effect of particles on the wall-normal and spanwise velocity fluctuations, resulting in a net reduction of turbulent kinetic energy. Regarding the impact on fluid properties, the effect of particles on the mean streamwise velocity and the mean temperature is found to be negligible at the volume fraction simulated. However, some modulation is observed in the fluid temperature variance. When the Stokes number increases to 60, the maximum temperature variance at the center of the channel increases by approximately 12% compared to the reference unladen flow. Conversely, when the Stokes number reaches 120, the maximum temperature variance decreases by approximately 6%. These changes in temperature variance are in line with the interplay between particle inertia and fluid turbulence, where enhanced mixing and heat transfer initially increase the variance, but the damping effect of particles subsequently reduces the turbulent kinetic energy and, thus, the temperature variance. Furthermore, the particle temperature variance is consistently larger than the fluid

variance and tends to reach its maximum value near the wall. This behavior can be attributed to particles being ejected from the wall region, where heat transfer is dominant, while retaining their temperature.

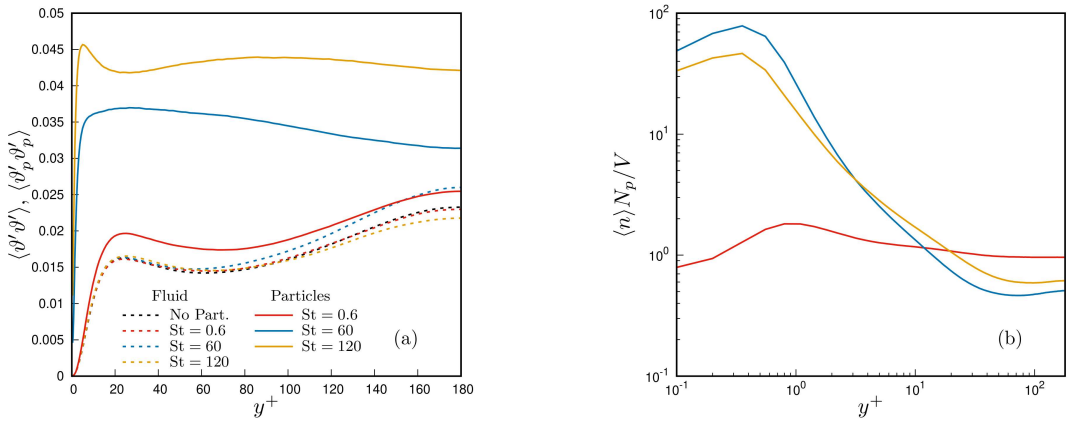

Figure 2. Forced convection in the two-way coupled particle-laden flow. Effect of the Stokes number, St: (a) fluid and particle temperature variance, (b) particle concentration.

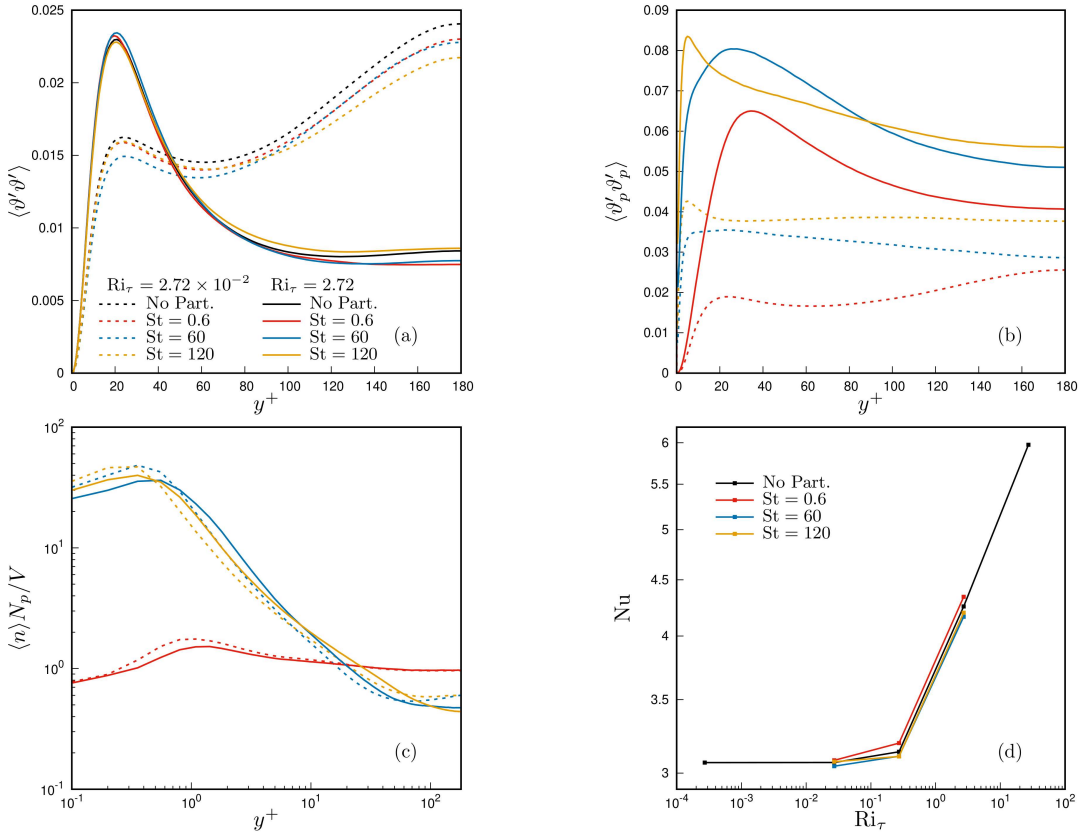

Figure 3. Mixed convection in the two-way coupled particle-laden flow. Effect of both the Stokes number, St, and the Richardson number, Ri_τ, on flow and particle statistics: (a) fluid temperature variance (b) particle temperature variance, (c) particle concentration, (d) average Nusselt number, $\mathrm{Nu} = 1/2\ (\partial\langle\vartheta\rangle/\partial y)_w$.

Figure 3 shows the influence of the Stokes number in the two-way coupled particle-laden channel flow when also natural convection is considered at $\mathrm{Ri}_\tau = 2.72 \times 10^{-2}$ and 2.72, representative of the

two flow regimes. Unlike the case of pure forced convection, particle feedback tends to damp the variance of the carrier flow temperature (figure 3(a)) for low Richardson numbers. This effect is milder for $\mathrm{Ri}_\tau > 1$. The enhancement of the wall-normal motion due to buoyancy increases particle temperature variance (figure 3(b)) due to a more frequent particle ejection from the wall region which also reduces the concentration peak near the wall (figure 3(c)), in particular at intermediate Stokes numbers. When the Richardson number exceeds one, the influence of natural convection becomes significant, enhancing heat transfer and increasing the Nusselt number (figure 3(d)). A non-monotonic modulation of the Nusselt number operated by particle inertia is observed.

5. Conclusions

This study provides a comprehensive exploration of mixed convection in turbulent particle-laden channel flows. The intricate dynamics revealed through eighteen simulations underscore the substantial influence of particle inertia on particle statistics, and a milder effect on fluid statistics due to the relatively low particle volume fraction considered. Notably, natural convection leads to distinct changes in flow structure and thermal characteristics as the friction Richardson numbers exceeds one. Turbophoresis is mainly observed under forced convection, with concentration profiles exhibiting non-monotonic behaviour as the Stokes numbers increase. The interplay of particle inertia and buoyancy in the presence of natural convection further modulates the Nusselt number, revealing a non-monotonic trend influenced by particle characteristics. These findings contribute valuable insights into the complex interactions between particles and fluid dynamics, essential for refining models in engineering applications, and into systems in which mixed convection play a pivotal role in heat transfer.

6. References

[1] Brandt L and Coletti F 2022 *Annu. Rev. Fluid Mech.* **54** 159-189
[2] Riley J J and Patterson Jr G S 1974 *Physics of Fluids* **17** 292-297
[3] Reeks M W 1983 *Journal of Aerosol Science* **14** 729-739
[4] Marchioli C and Soldati A 2002 *Journal of Fluid Mechanics* **468** 283-315
[5] Perrone D, Kuerten J, Ridolfi L and Scarsoglio S 2023 *International Journal of Multiphase Flow* **165** 104489
[6] Elghobashi S 1994 *Applied Scientific Research* **52** 309-329
[7] Kuerten J G M, van der Geld C W M and Geurts B J 2011 *Physics of Fluids* **23** 123301
[8] Carbone M, Bragg A D and Iovieno M 2019 *Journal of Fluid Mechanics* **881** 679-721
[9] Harish R and Sivakumar R 2021 *Powder Technology* **378** 303-316 ISSN 0032-5910
[10] Pirozzoli S, Bernardini M, Verzicco R and Orlandi P 2017 *Journal of Fluid Mechanics* **821** 482-516
[11] Maxey M R and Riley J J 1983 *Physics of Fluids* **26** 883-889
[12] Morsi S A and Alexander A J 1972 *Journal of Fluid Mechanics* **55** 193-208
[13] Ranz W E and Marshall Jr W R 1952 *Chemical Engineering Progress* **48** 173-180
[14] Kim J, Moin P and Moser R 1987 *Journal of Fluid Mechanics* **177** 133-166
[15] Kleiser L and Schumann U 1979 *Notes on Numerical Fluid Mechanics* **2** 165-173
[16] Canuto C, Hussaini M Y, Quarteroni A and Zang T A 1988 *Spectral Methods in Fluid Dynamics* (Heidelberg: Springer) ISBN 978-3-540-52205-8
[17] Thual O 1986 *Transition vers la turbulence dans des systèmes dynamiques apparentés a la convection* (Ph.D Thesis, Universitè de Nice-Sophia Antipolis)
[18] Sid S, Dubief Y and Terrapon V E 2015 *8th International Conference on Computational Heat and Mass Transfer* (Istanbul, Turkey) p 190

Acknowledgments

The authors acknowledge the computer resources provided by CINECA under the ISCRA initiative, project HP10CIUF9S. Additional resources were provided by HPC@POLITO, a project of Academic Computing within DAUIN at the Politecnico di Torino (http://www.hpc.polito.it).